RSC Advances

PAPER

View Article Online
View Journal | View Issue

Cite this: *RSC Adv.*, 2026, **16**, 27579

Magnetite hybrid hydrogel of xanthan gum and poly(*N*-hydroxyethyl acrylamide): a cytocompatible vehicle for sustained oral dual delivery of 5-fluorouracil and curcumin

Ngeleja S. Hamis, Amos Luanda * and John J. Makangara

In the present work, a pH-sensitive magnetite hybrid hydrogel was prepared as a potential oral dual drug delivery system. The magnetite (Fe_3O_4) nanoparticles were *in situ* incorporated into the pH-sensitive hydrogel containing xanthan gum (XG) and poly(*N*-hydroxyethyl acrylamide) (PAHEA), which was prepared *via* a free radical polymerization. Ultimately, anticancer drugs, namely 5-fluorouracil (5-FU) and curcumin (CUR), were successfully loaded into the developed magnetite hybrid hydrogel. The swelling studies showed minimal swelling of the system at pH 1.2 and significant swelling at pH 7.4. The drug quantities incorporated per gram of dry magnetite hybrid hydrogel were determined to be 48.2 ± 0.8 mg g^{-1} for 5-FU and 38.5 ± 0.5 mg g^{-1} for CUR. The sequential drug release studies revealed that the prepared dual drug delivery system retained the incorporated drugs in the simulated gastric environment and significantly released them in the simulated intestinal environment of the gastrointestinal tract. The drug release mobility at pH 7.4 followed non-Fickian diffusion for 5-FU and Super Case II transport for CUR. The cytotoxicity investigation of the magnetite hybrid hydrogel, with and without drugs, using the MTT assay towards normal cells (MCF-10A) showed good cytocompatibility, with cell viability exceeding 75%. However, the drug-loaded magnetite hybrid hydrogel showed remarkable cytotoxicity against cancer cells (MCF-7), with cell viability being below 35%. These results suggest that the prepared magnetic hybrid hydrogel could serve as a promising site-specific drug delivery system for the prolonged oral dual release of 5-FU and CUR in cancer therapy.

Received 3rd March 2026
Accepted 17th May 2026

DOI: 10.1039/d6ra01832g

rsc.li/rsc-advances

1. Introduction

The release of dual drugs in cancer therapy is a preferred treatment approach that demonstrates favorable therapeutic efficacy.[1] The injection method is a common strategy for the administration of anticancer drugs, but it is associated with side effects, which can be mitigated by changing the drug administration route, particularly the use of oral drug administration.[2] Several studies addressed the combination release of anticancer drugs from delivery systems *via* oral administration.[3,4] Recently, the development of controlled, targeted, and sustained drug delivery systems has captured the interest of many researchers due to their potential to improve therapeutic efficacy. These systems offer benefits, such as delivering desired therapeutic effects at lower doses and reducing toxicity and related side effects compared with traditional dosage forms. In this context, among the favorable drug delivery systems is the use of hydrogel-based materials.

Hydrogels are hydrophilic, crosslinked polymeric materials in a three-dimensional structure that can absorb large quantities of water or biological fluids and retain their polymer network in the swollen state.[5] The previous studies indicate that hydrogels are crucial polymer matrix materials across multiple fields of biomedical applications, such as drug delivery,[6] tissue engineering scaffolds,[7] wound healing, and bioprinting.[8] In drug delivery applications, pH-sensitive hydrogels are of great interest due to their ability to release both single and multiple drugs in a controlled, targeted and sustained manner.[9,10] Additionally, these materials can be formed from both natural and synthetic polymers containing acidic, basic or neutral functional groups, or a combination of all.[11,12] However, based on the degradability, biocompatibility, non-toxicity and low cost, natural polymers are preferred in designing pH-sensitive hydrogels. Specifically, polysaccharides, as natural polymers, have been extensively used to prepare pH-sensitive drug delivery systems, as they can modulate the gut microbiota and improve the intestinal microenvironment, thereby enhancing intestinal immunity.[13,14]

Xanthan gum (XG) is an anionic natural polysaccharide produced by the bacterium *Xanthomonas campestris*. It is a branched polysaccharide unit of D-glucoronic acid, D-mannose

Department of Chemistry, College of Natural and Mathematical Sciences, The University of Dodoma, P.O. Box 338, Dodoma, Tanzania. E-mail: amoscosmasl@gmail.com

and D-glucose in a 1 : 2 : 2 ratio.[15] It is commonly used in food and pharmaceutical applications. XG can be crosslinked with both chemical and physical crosslinking agents, such as *N*,*N*′-methylenebisacrylamide (MBA) and calcium ions respectively.[16,17] The pH-sensitive XG-based hydrogels can be readily prepared in a few steps under mild conditions, making them widely studied, particularly for drug delivery applications. The presence of carboxylic acid functional groups in the structure of XG helps to resist swelling of the hydrogels in an acidic medium of the gastric conditions, while they can swell considerably in an alkaline medium of intestinal conditions. In this context, they are extensively studied as pH-sensitive systems for oral drug delivery.

Hydrogels made solely from native polysaccharides have limitations, such as poor mechanical strength and uncontrolled drug release.[18] These limitations can be mitigated by adding an appropriate amount of synthetic polymers and incorporating nanoparticles, which collectively improve the properties and functionalities of the hydrogels. In particular, nanocomposite hybrid hydrogel exhibits the combined properties of polymer and nanoparticles. Various nanoparticles, such as graphene oxide, hydroxyapatite, titanium oxide, metal nanoparticles and iron oxide have been utilized for the preparation of magnetite hybrid hydrogel to improve the properties and performance of the hydrogels.[19,20] The extent of improvement may depend on the type of nanoparticles. Several studies have used magnetite (Fe_3O_4) nanoparticles to form magnetite-hybrid hydrogels due to their unique properties, including magnetic responsiveness, low toxicity, and compatibility with many polymers.[21–23] Additionally, Fe_3O_4 nanoparticles within a gel matrix facilitate prolonged drug release at the desired site.

In continuation of our previous research on drug delivery applications of hydrogel-based materials, the present study aims to develop a magnetite hybrid hydrogel as a pH-sensitive delivery system for the oral dual release of 5-fluorouracil (5-FU) and curcumin (CUR). The details of 5-FU and CUR have been provided in our previous studies.[24–26] The pH-sensitive properties of the developed polymer matrix material were dominated by the XG. The XG was modified by grafting it with poly(*N*-hydroxyethyl acrylamide) (PHEA) and subsequently incorporating Fe_3O_4 nanoparticles to enhance its mechanical strength and overall performance. However, XG significantly contributes to a favorable release profile by protecting the loaded drugs from acidic conditions and releasing them in intestinal conditions. The novelty of this work lies in both the materials used and the drug release strategy compared with previously reported magnetite-based hydrogels. In brief, integrating xanthan gum with poly(*N*-hydroxyethyl acrylamide) provides a unique balance between hydrophilicity and structural stability, results in improving physicochemical properties and functionality. Furthermore, the incorporation of Fe_3O_4 nanoparticles plays a dual role by enhancing network integrity and introducing additional interaction sites for drug molecules, thereby improving loading efficiency and modulating release behavior. At the structural level, Fe_3O_4 nanoparticles serve as additional physical crosslinking points within the polymer network, thereby enhancing mechanical stability, reducing polymer chain mobility, and facilitating a slower and sustained release profile. Additionally, the polymer matrix developed in the present study demonstrates a pH-responsive, sustained, and controlled release profile *via* a sequential release approach, which is uncommon in the literature, particularly for dual release of anticancer drugs, since several reported systems employed non-sequential oral drug release strategies.

2. Materials and methods

2.1. Materials

Xanthan gum and ammonium peroxodisulphate (98%) were obtained from Sisco Research Laboratory Pvt. Ltd, Mumbai, India. Iron(II) chloride tetrahydrate ($FeCl_2 \cdot 4H_2O$), iron(III) chloride hexahydrate ($FeCl_3 \cdot 6H_2O$), *N*,*N*′-methylenebisacrylamide (99%), *N*-hydroxyethyl acrylamide (HEA), 5-fluorouracil (99%), and curcumin (99%) were purchased from Aldrich Chemical Company Inc., USA. MCF-7 and MCF-10A cell lines were received from Infinite Biotech Institute of Research and Analytics, Mumbai, India. All reagents were of analytical grade and were used without further purification.

2.2. Preparation of hydrogel

An aqueous solution of XG (0.25% w/v) was prepared at room temperature with the help of a magnetic stirrer. To it, a known amount of HEA (9.6, 19.1 and 28.9 mmol) was added and thoroughly stirred to get a homogenous solution. Next, 1 mL of APS (0.066 mmol) and 1 mL of MBA (0.097 mmol) were added while stirring continuously. The obtained homogeneous solution was placed in a domestic microwave and irradiated at 80 W for 25 s. To eliminate by-products and unreacted components, the obtained hydrogels were vigorously washed with acetone and distilled water. Then, dried at 50 °C to constant weight. The hydrogels made by adding 9.64, 19.12 and 28.92 mmol of HEA are coded XG-*g*-PHEA-1, XG-*g*-PHEA-2 and XG-*g*-PHEA-3 respectively. The grafting efficiency (GE) of the obtained hydrogels was determined using eqn (1). The hydrogel with the highest GE was selected for further modification.[27]

$$\mathrm{GE} = \frac{(S_1 - S_2)}{S_3} \times 100 \quad (1)$$

where S_1, S_2, and S_3 stand for the weights of the hydrogel, XG and HEA respectively.

2.3. Preparation of magnetite hybrid hydrogel

A previously reported method[28] was followed for the *in situ* incorporation of Fe_3O_4 nanoparticles into the hydrogel. In brief, approximately 0.6 g of dry hydrogel was immersed in 100 mL of an aqueous solution containing 5.8 g of $FeCl_3 \cdot 6H_2O$ and 2.1 g of $FeCl_2 \cdot 4H_2O$. The hydrogel was allowed to equilibrate overnight. The yellow-orange, swollen gel containing iron(II) and iron(III) ions was transferred to 100 mL of 0.5 M ammonium solution and left overnight. The magnetite hybrid hydrogel obtained was designated XG-*g*-PHEA-2/Fe_3O_4. It was thoroughly washed with distilled water and dried at 50 °C to constant weight.

2.4. Characterization

The prepared materials were characterized using a Fourier Transform Infrared (FTIR) spectrophotometer (Bruker Alpha, Germany) at a resolution of 2 cm^{-1}. The morphological features were investigated using a scanning electron microscope (SEM), Carl Zeiss Sigma (Germany), at a voltage of 20.00 kV. Energy-dispersive X-ray spectroscopy (EDS) confirmed elemental compositions of the materials. The powder X-ray diffractometer, AXS D8, from Bruker Ltd, Germany, at a recording rate of 2° min^{-1} with a resolution of 0.0001° was used to evaluate the nature of the materials. The magnetization of the magnetite hybrid hydrogel was recorded at room temperature using a vibrating sample magnetometer (VSM) 7410S, Lakeshore Company, USA, with an applied magnetic field of 1.5 T in the range −20 000 to +20 000 Oe and a sensitivity of 10^{-6}.

2.5. Swelling behavior

The known weights of the dry samples were placed separately in beakers containing sufficient buffer solutions at pH 1.2 and 7.4 at room temperature. After a certain interval, the weights of the swollen samples were recorded. Weight recording was carried out until the samples attained equilibrium swelling. The swelling ratio (SR) in g g^{-1} was calculated using eqn (2).[24]

$$SR = \frac{G_t - G_0}{G_0} \quad (2)$$

where G_0 is the initial weight of the gel and G_t is the weight of the swollen gel at a predetermined interval.

2.6. Drug loading efficiency (DLE) and drug entrapment efficiency (DEE)

In triplicate, the loading and entrapment of the 5-FU and CUR were performed as reported in a previous study.[26] Briefly, a dry sample of known weight was placed in CUR solution (0.5 mg mL^{-1} in ethanol–water (1 : 1)) at room temperature for 24 h in the dark to protect CUR from photodegradation. Then, the remaining CUR solution was measured at λ_{max} 429 nm using a Shimadzu UV1900 UV-visible spectrophotometer. A similar procedure was adapted to load 5-FU, but in an aqueous medium (0.5 mg mL^{-1}) at room temperature. The absorbance of the remaining 5-FU solution was measured at λ_{max} 266 nm. To ensure that the actual value of CUR was obtained in the final drug-loaded sample, the same 5-FU solution was measured at λ_{max} 429 nm to detect any traces of CUR. The DLE (mg g^{-1}) and the percentage of DEE were determined using eqn (3) and (4) respectively,[26] and the results obtained are expressed as the mean ± standard deviation.

$$DLE = \frac{\text{Weight of the drug in the system}}{\text{Weight of system}} \quad (3)$$

$$DEE = \frac{\text{Weight of the drug in the system}}{\text{Initial weight of the drug}} \times 100 \quad (4)$$

2.7. *In vitro* drug release study

The release of 5-FU and CUR from the drug-loaded samples into the dissolution medium was performed using procedures similar to those described in our previous study, with a few modifications.[25] Briefly, a sequential drug release study was performed by transferring the sample from a buffer solution of pH 1.2, as a simulated gastric fluid, after 2 h, to a buffer solution of pH 7.4, as a simulated intestinal fluid. The cumulative drug release (CDR) was calculated as follows:

$$CDR = \frac{\text{Weight of drug released from the system}}{\text{Weight of the drug loaded to the system}} \times 100 \quad (5)$$

2.8. Cytotoxicity study

The cytotoxicity study was performed for both blank and drug-loaded magnetite hybrid hydrogels using the MTT assay against MCF-10A and MCF-7 cell lines in triplicate, as reported elsewhere with minor modification, and the cell viability was calculated using eqn (9).[29,30] In brief, cells were cultured in 96-well plates at a density of 0.1×10^5 cells per well and incubated for 24 h to allow attachment. The stock solution (0.5 mg mL^{-1}) of the blank nanocomposite was prepared in dimethyl sulfoxide, and appropriate dilutions were made from it to obtain a set of predetermined concentrations. For drug-loaded samples, the corresponding drug content was calculated. Cells were treated with different concentrations of the samples (20, 40, 60, 80, and 100 μg mL^{-1}) for 24 h. After incubation, MTT solution (0.5 mg mL^{-1}) was added, and the cells were incubated for an additional 4 h. The resulting formazan crystals were dissolved in dimethyl sulfoxide, and absorbance was measured at 540 nm using a microplate reader.

$$\text{Cell viability} = \frac{\text{Absorbance of sample}}{\text{Absorbance of control}} \times 100 \quad (6)$$

2.9. *In vitro* degradation study

Under slow stirring, a known weight of the sample (W_a) was immersed in a sufficient volume of phosphate buffer solution of pH 7.4 at 37 °C. At a specified time, the weight of the sample (W_b) was recorded and the weight loss was determined using eqn (7).[31]

$$\text{Weight loss}(\%) = \frac{W_a - W_b}{W_a} \times 100 \quad (7)$$

2.10. Statistical analysis

The statistical analysis of the obtained experimental data was performed using OriginPro 2022 v.9.9.0.225 (SR1) software. All experiments were performed in triplicate ($n = 3$), and the results are expressed as mean ± standard deviation. The best-fitting mathematical model was determined by comparing the correlation coefficient (R^2) values.

3. Results and discussion

3.1. Preparation of magnetite hybrid hydrogel

Polysaccharide-based matrices can interact with different metal cations, including hematite. This is facilitated by the existence

of various functional groups, including amine, amide, hydroxyl and carboxylic acid groups in the polymer network.[32] In the present study, the grafting of PHEA onto the XG backbone facilitates the easy binding of Fe^{2+} and Fe^{3+} ions *via* coordinate bonds. Similarly, the carboxylate (COO^-) groups from XG could bind iron ions *via* electrostatic interactions. The hydrogel exhibited promising capacity to bind iron ions and was therefore used as a template for the *in situ* incorporation of Fe_3O_4 nanoparticles *via* oxidation induced by an NH_4OH solution. In brief, during the formation of the magnetite hybrid hydrogel, the loading of the neat hydrogel with Fe^{2+}/Fe^{3+} ions could be followed by the visual turning of the white swollen gel to yellow-

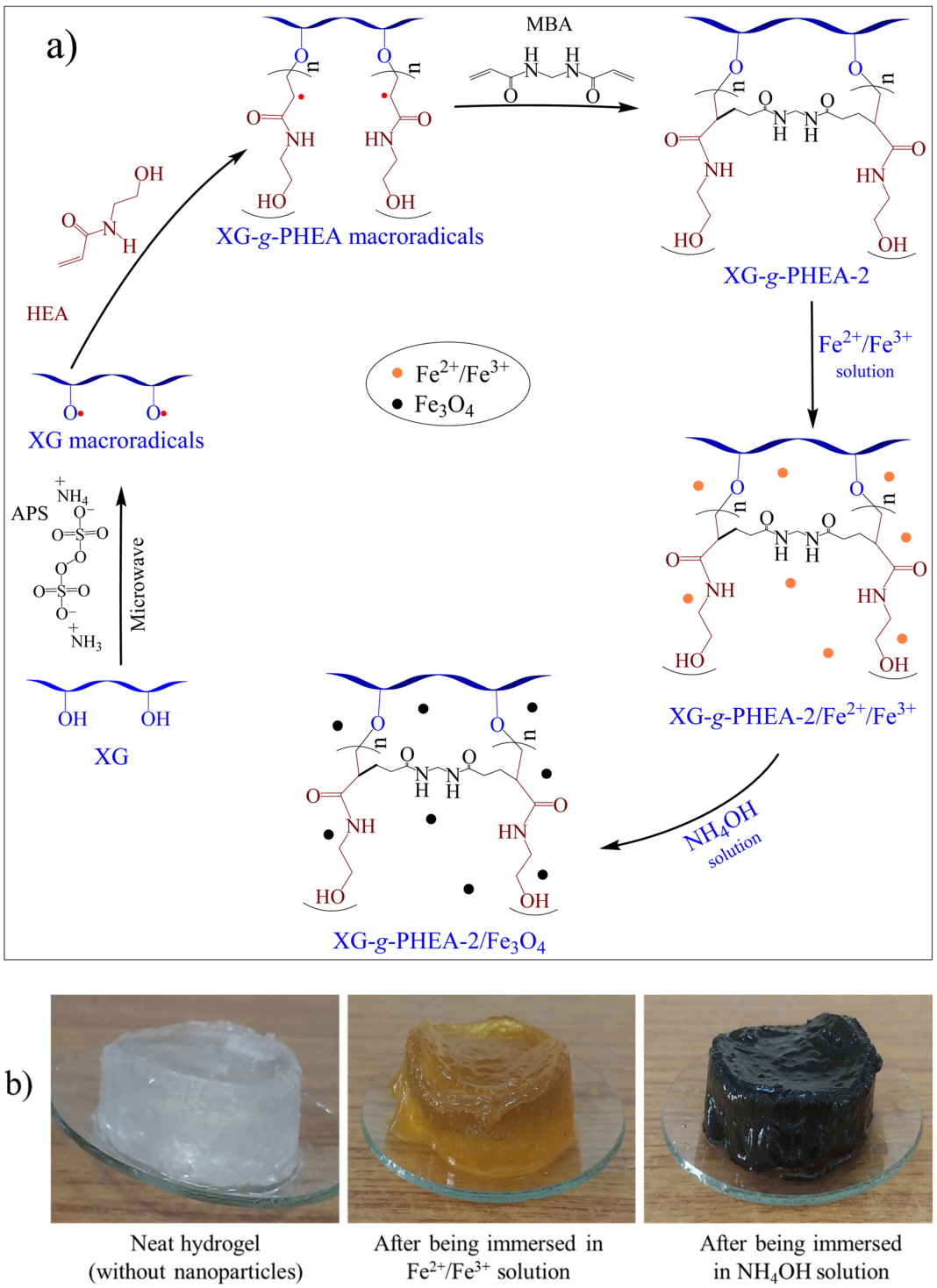

Fig. 1 Representation of the (a) mechanism of formation of the magnetite hybrid hydrogel and (b) visual appearance of the hydrogel at different preparation steps.

Table 1 Gel fraction of the prepared polymer matrix materials[a]

Sample code	HEA (mmol)	GE (%)
XG-*g*-PHEA-1	9.6	80.7
XG-*g*-PHEA-2	19.1	96.5
XG-*g*-PHEA-3	28.9	92.2

[a] XG = 0.25% w/v, APS = 0.066 mmol, MBA = 0.097 mmol.

orange, as illustrated in Fig. 1. The color of the hydrogel was retained after washing it with distilled water, suggesting that Fe^{2+}/Fe^{3+} ions strongly bound to the hydrogel. Upon immersion of the swollen gel loaded with iron ions in an NH_4OH solution, the hydrogel's yellow-orange color rapidly changed to black. This indicates that Fe_3O_4 nanoparticles form spontaneously *via* oxidation. Shruthi S. and Vishalakshi B. observed similar changes during the preparation of cellulose fiber-based magnetic nanocomposite.[28]

3.2. Grafting efficiency

The results of the GE (Table 1) indicate that the grafting of HEA onto XG chains was effective, attributed to microwave irradiation, which favors reaction conditions and compatibility of the reacting components.[33] The GE is maximum when 19.1 mmol of HEA was used, indicating that at this amount, the maximum amount of HEA was utilized by grafting with XG. Below this amount, the GE was low due to the insufficient number of HEA units for grafting. Similarly, beyond 19.1 mmol of HEA, the GE decreased due to excess ungrafted HEA that remained unreacted or reacted to form homopolymers without grafting. In this context, the hydrogel with the highest GE (XG-*g*-PHEA-2) was selected as an ideal polymer material for further studies.

3.3. Characterization

For native XG, the FTIR spectrum displays a distinct broad band at 3416 cm^{-1} due to the vibrations of the –OH group, and 2922 cm^{-1} and 2851 cm^{-1}, which correspond to –CH. The bands at 1729 cm^{-1}, 1641 cm^{-1}, 1382 cm^{-1}, and 1025 cm^{-1} are attributed to the C=O stretching vibrations of alkyl esters, the asymmetric stretching of $–COO^-$ groups, C–H bending, and C–O stretching of the C–OH group, respectively.[34,35] The XG-*g*-PHEA-2 hydrogel spectrum exhibits a broad band at 3424 cm^{-1} due to the overlapping of the stretching vibrations of the –OH group of XG and the –NH amide group of PHEA. The band at 1454 corresponds to the –C–N stretching vibration and 1380 cm^{-1} is due to the overlap of the –C–N stretching vibration of HEA and the –CH bending band of the XG methyl group.[35] The bands in the FTIR spectrum of the XG-*g*-PHEA-2/Fe_3O_4 resemble to that of the neat hydrogel, but with the appearance of the weak band at 463 cm^{-1} due to Fe–O, confirming the presence of Fe_3O_4 nanoparticles in the gel structure.[36] The pure 5-FU displayed the stretching vibration bands for –NH at 3132 cm^{-1}, –CH at 2922 cm^{-1} and 2822 cm^{-1}, –C=C– cyclic aliphatic at 1662 cm^{-1}, multi-substituted pyrimidine moiety at 1427 cm^{-1} and –C–F at 1248 cm^{-1}.[37] The FTIR spectrum of the pure CUR exhibits the stretching vibration bands for –OH at 3506 cm^{-1}, –CH at 2924 cm^{-1} and 2851 cm^{-1}, aromatic –C=C– at 1505 cm^{-1} and –C–O at 1025 cm^{-1}.[38,39] The drug-loaded polymer gels exhibit overlapping bands of both drugs and matrices, which makes the interpretation difficult. However, such drastic changes indicate the successful incorporation of the drug molecules into the polymer network (Fig. 2).

The morphological structure of XG-*g*-PHEA-2/Fe_3O_4 changed when compared to XG-*g*-PHEA-2. Upon incorporating Fe_3O_4 nanoparticles into the gel structure, the surface of the obtained magnetite hybrid hydrogel became rougher than the neat hydrogel, as depicted in Fig. 3a and b. Additionally, the magnetite hybrid hydrogel exhibits heterogeneous pore distribution with a large number of pores. The pore size was estimated from SEM images using ImageJ. The scale was calibrated using the embedded scale bar, and pore diameters were measured manually on randomly selected pores. The estimated average pore size of the neat hydrogel is approximately 3.0 ± 1.7

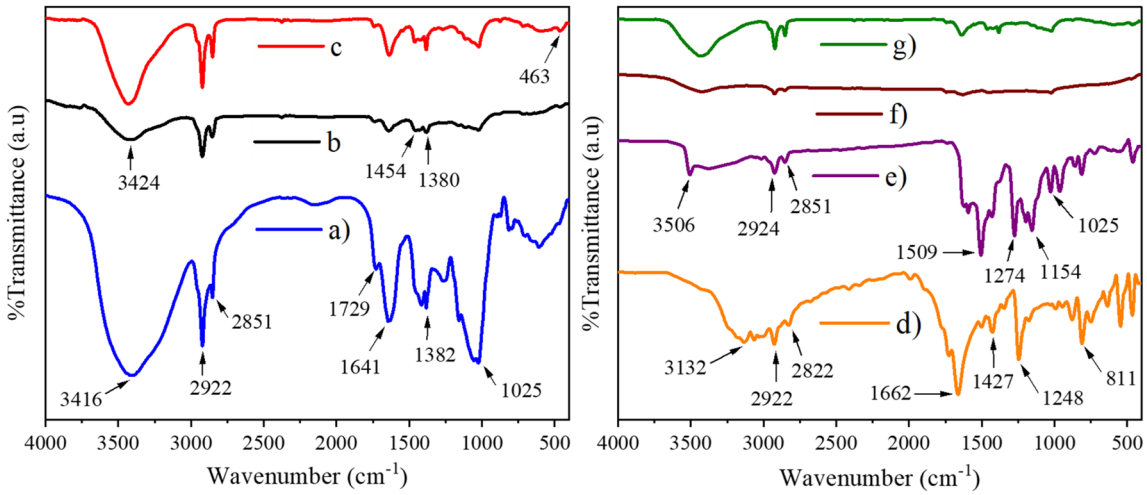

Fig. 2 FTIR spectra of (a) XG (b) XG-*g*-PHEA-2 (c) XG-*g*-PHEA-2/Fe_3O_4 (d) 5-FU (e) CUR (f) XG-*g*-PHEA-2@5-FU/CUR and (g) XG-*g*-PHEA-2/Fe_3O_4@5-FU/CUR.

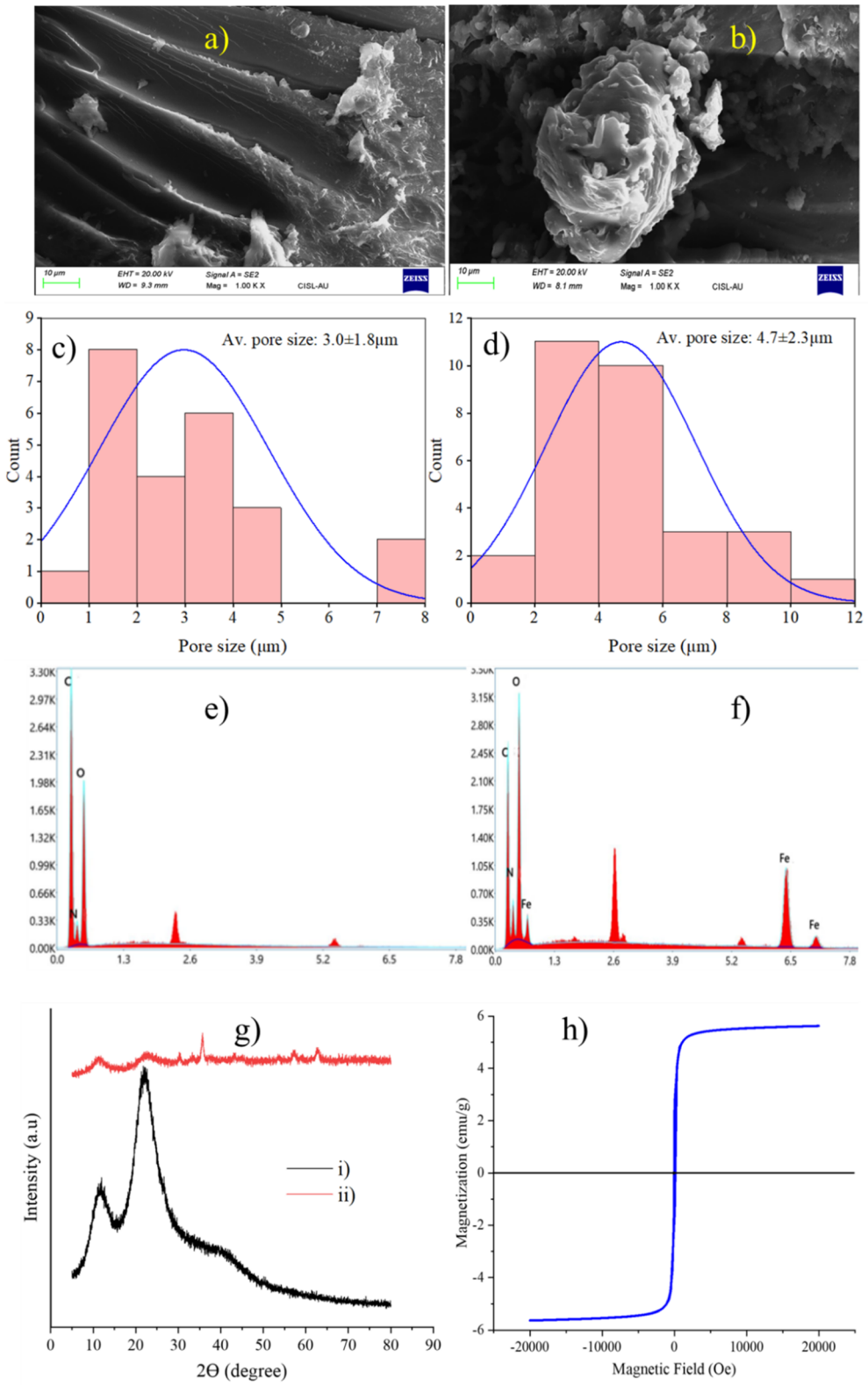

Fig. 3 FE-SEM images of (a) XG-*g*-PHEA-2 and (b) XG-*g*-PHEA-2/Fe_3O_4; pore size distribution curves of (c) XG-*g*-PHEA-2 and (d) XG-*g*-PHEA-2/Fe_3O_4; EDS spectra of (e) XG-*g*-PHEA-2 and (f) XG-*g*-PHEA-2/Fe_3O_4; (g) PXRD patterns of (i) XG-*g*-PHEA-2 and (ii) XG-*g*-PHEA-2/Fe_3O_4; (h) magnetization curve of XG-*g*-PHEA-2/Fe_3O_4.

μm (Fig. 3c). The incorporation of Fe_3O_4 nanoparticles appears to modify the pore architecture, resulting in a more compact, heterogeneous network with an estimated average pore size of 4.7 ± 2.3 μm (Fig. 3d). Further, successful incorporation of Fe_3O_4 nanoparticles within the polymer network was also confirmed by the appearance of the Fe peak in the EDS spectrum of the XG-*g*-PHEA-2/Fe_3O_4 in addition to all essential elements present in both magnetite hybrid hydrogel and the neat hydrogel spectra (Fig. 3e and f).

From the PXRD spectra (Fig. 3g), the neat hydrogel displays two strong peaks at 2θ ranging from 10 to 30, suggesting a semi-crystalline nature of the hydrogel. The intensities of these peaks are significantly decreased in the magnetite hybrid hydrogel, possibly due to the interactions between the polymer network and Fe_3O_4 nanoparticles. The peak positions at 2θ values 30.45, 35.77, 43.36, 57.27, and 62.87 correspond to an inverse spinel structure of Fe_3O_4 nanoparticles.[32] In addition, the crystallite size of Fe_3O_4 nanoparticles embedded in a polymer network was estimated from PXRD patterns using the Debye Scherrer equation, as follows:

$$D = \frac{K\lambda}{\beta \cos \theta} \quad (8)$$

where D is the crystallite size in nm, K is the dimensionless Debye Scherrer constant (0.9 for spherical nanoparticles), λ is the wavelength of the X-ray source (for this study is 0.154 nm), β is the half-width of the diffraction peak in radians, and θ is the Bragg diffraction angle in radians. The results confirmed that Fe_3O_4 was in nanoscale with an estimated crystallite size of 12.4 nm. This suggests the high surface area of Fe_3O_4 particles within the polymer matrix, which enhances interactions with the polymer chains and thereby influences drug-loading capacity. The magnetization curve of the magnetite hybrid hydrogel (Fig. 3h) exhibits superparamagnetic behavior, with a coercivity of 5.6 emu g^{-1}, making it suitable for controlled drug release under magnetic fields. Sivudu *et al.*, reported similar findings from the polyacrylamide magnetite hybrid hydrogel with a magnetization value of 4 emu g^{-1}.[32]

Generally, Fe_3O_4 nanoparticles impart magnetic responsiveness to the system, offering the potential for externally guided targeting or stimuli-responsive drug release. Although this aspect was not explored in the present study, it represents a significant advantage over conventional hydrogels and provides a rationale for including magnetite nanoparticles in the system design. However, it is acknowledged as a limitation of the study and remains an important direction for future investigation.

3.4. Swelling study

The effect of swelling medium and the Fe_3O_4 nanoparticles on the swelling behavior of the designed polymer matrices was evaluated and the results are graphically displayed in Fig. 4. Each selected swelling medium has a significant meaning. In brief, ethanol–water (1 : 1) was used for drug loading, while buffer solutions of pH 1.2 and 7.4 were used for drug release studies. The lowest swelling obtained in ethanol–water (1 : 1) is attributed to the change in hydrophilicity of the medium. The gel materials do not swell in various ordinary organic solvents, including ethanol. In this context, mixing ethanol with water reduces the swelling capacity of the matrices, resulting in lower water uptake. The highest SR was observed in a buffer solution at pH 7.4, which is close to neutral. At this pH, the COO^- groups in XG remain ionized, leading to electrostatic repulsion. Therefore, the polymer network expands, facilitating the diffusion of the swelling medium into the matrices. Unlike at pH 1.2, the COO^- groups protonate, reducing electrostatic repulsion and thereby affecting the expansion of the gel matrices and overall swelling capacity. Moreover, the swelling profile shows a decrease in SR for the gel containing Fe_3O_4. This trend is attributed to the presence of Fe_3O_4, which increases cross-linking density through interactions between the Fe_3O_4 nanoparticle gel matrices.[40] In brief, incorporating Fe_3O_4

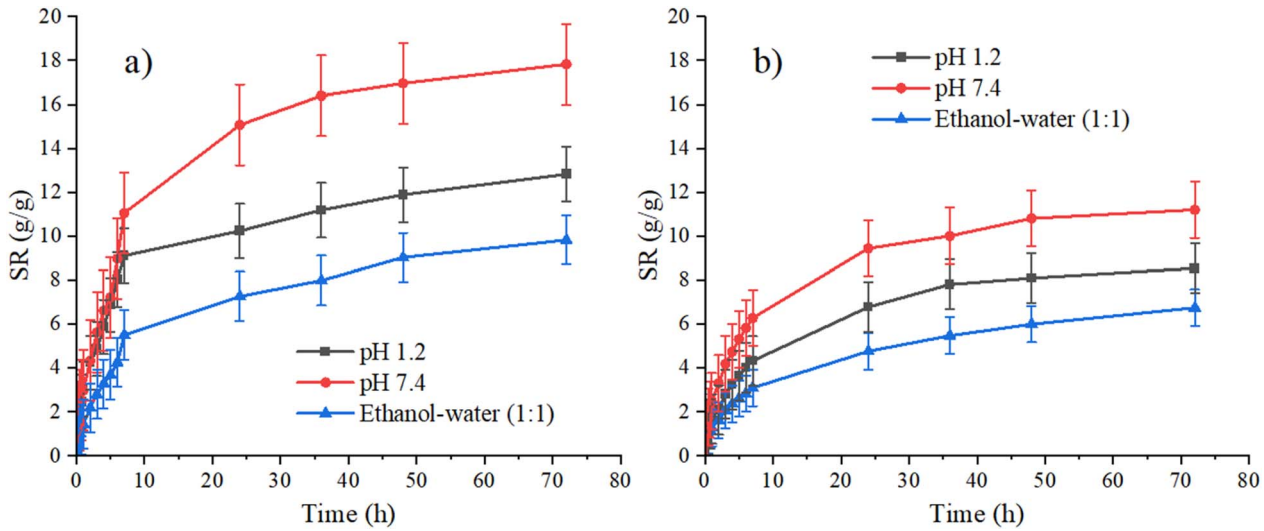

Fig. 4 Swelling behavior of (a) XG-*g*-PHEA-2 and (b) XG-*g*-PHEA-2/Fe_3O_4. Error bars represent standard deviation (n = 3).

Table 2 Drug loading and entrapment efficiencies of the prepared polymer matrix materials

	DLE (mg g^{-1})		DEE (%)	
Sample codes	5-FU	CUR	5-FU	CUR
XG-*g*-PHEA-2	39.1 ± 0.6	35.4 ± 0.2	78.9 ± 1.3	71.0 ± 0.4
XG-*g*-PHEA-2/Fe_3O_4	48.2 ± 0.8	38.5 ± 0.5	92.4 ± 1.7	81.3 ± 1.0

nanoparticles plays an important role in modulating the structure and functionality of the hydrogel. Fe_3O_4 nanoparticles can interact with the hydroxyl and amide groups of XG and PHEA, possibly *via* coordination bonding. These interactions serve as additional physical crosslinking points, contributing to a more interconnected and stable polymer network. The presence of well-dispersed nanoparticles in a polymer network usually introduces microstructural heterogeneity within the matrix, generating localized free volume and hydrophilic regions that facilitate water penetration. However, in this study, incorporating Fe_3O_4 nanoparticles into the gel structure led to a slight decrease in water uptake, indicating increased crosslinking density. Although direct measurement of crosslinking density was not performed, the observed swelling behavior provides indirect evidence of network structure. The slight decrease in swelling for the nanocomposite hydrogel suggests a balance between nanoparticle-induced crosslinking and the formation of additional free volume within the polymer network. This structural feature is important in controlling drug diffusion and overall release behavior.

3.5. Loading and release of drugs

An ethanol–water (1 : 1) mixture was used to load the CUR, facilitating its solubility. Unlike 5-FU, which is practically soluble in an aqueous medium, it was dissolved in water. The highest DLE and DEE values were observed for the magnetite hybrid hydrogel compared with its corresponding neat gel, as shown in Table 2. For both samples, 5-FU outperforms the neat gel in terms of loading and entrapment efficiencies. The primary driving force for loading both 5-FU and CUR into the gel samples can be related to the hydrogen bonding (Fig. 5). However, the extent of the drug to form hydrogen bonding with polymer matrices depends on the nature of the drug and the available functional groups. In this context, hydrogen bonding between 5-FU and the polymer network is most likely to dominate that between CUR and the polymer network. Further, the higher drug concentration in the magnetite hybrid hydrogel than in the neat gel was due to the presence of Fe_3O_4 nanoparticles in the gel structure, which provided additional interaction sites for drug entrapment, thereby increasing the loading efficiency.[40] Briefly, Fe_3O_4 nanoparticles possess a high specific surface area, which provides additional binding or adsorption sites for drug molecules. These interactions may include hydrogen bonding and weak electrostatic interactions (not shown), thereby contributing to the increased drug-loading capacity observed in the nanocomposite hydrogel.

The 5-FU and CUR sequential release profiles at pH 1.2 and pH 7.4 were studied for 48 h at 37 °C, and the obtained results are graphically displayed in Fig. 6a. At pH 1.2, the cumulative release was below 25% for 5-FU and 10% for CUR during 2 h. When the samples transferred into pH 7.4, a significant release of approximately 3 times for 5-FU and 4 times for CUR was observed during the first 2 h. This trend can be related to the

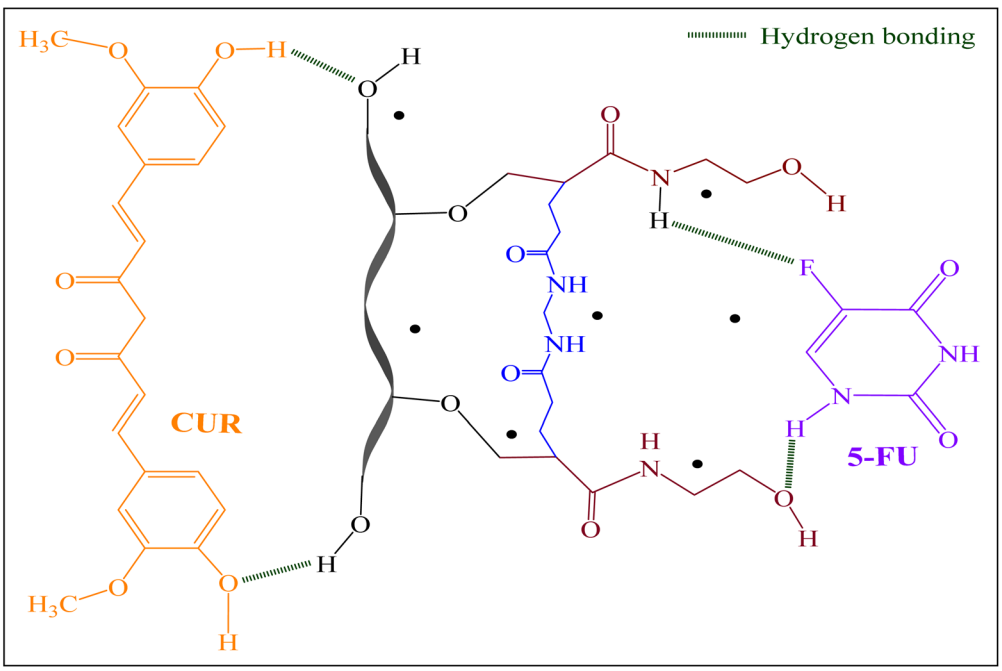

Fig. 5 Intermolecular interactions between XG-*g*-PHEA-2/Fe_3O_4 with 5-FU and CUR.

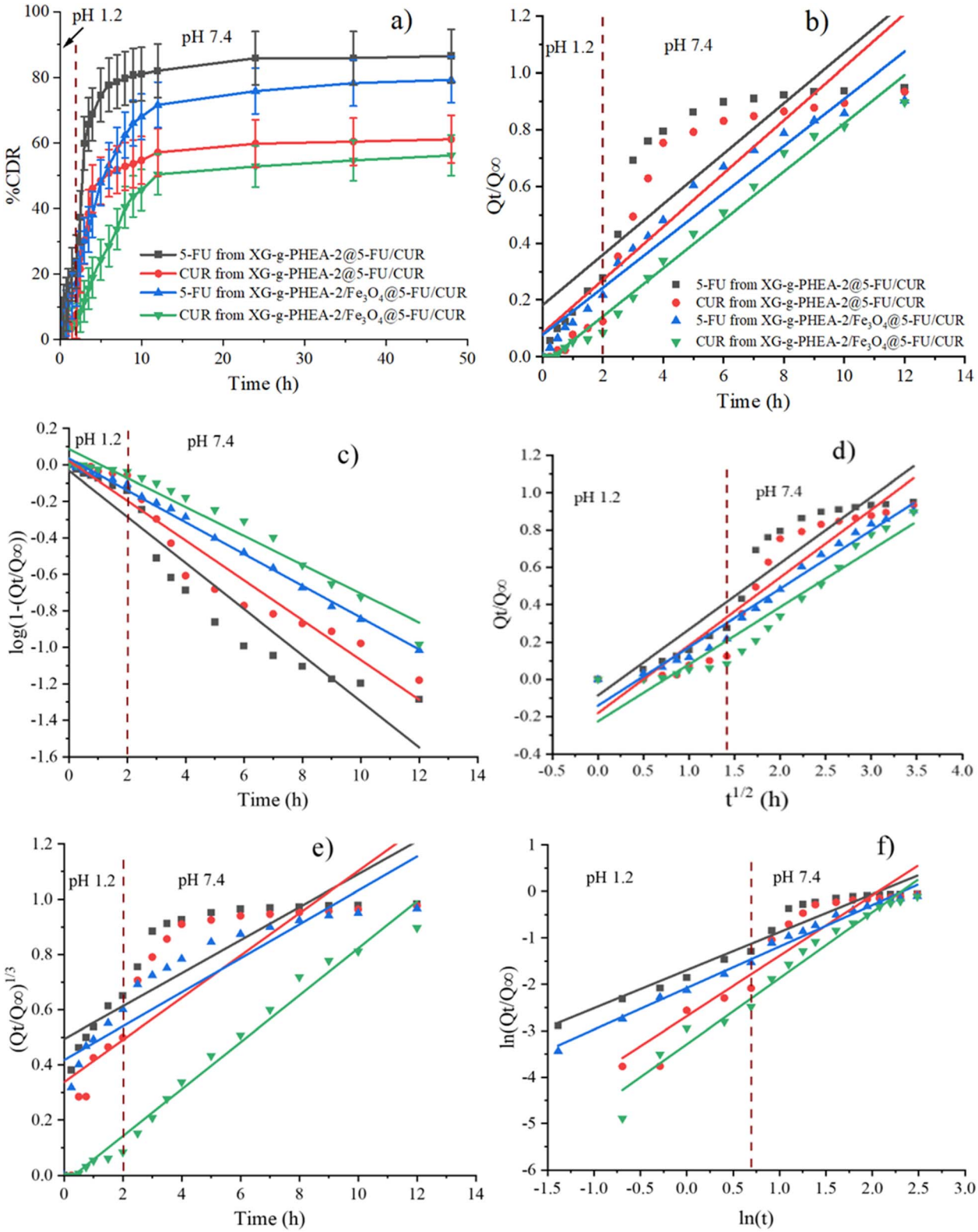

Fig. 6 Graphs displaying (a) *in vitro* drug release profile; fits of drug release data to (b) zero order kinetic, (c) first order kinetic, (d) Higuchi square root, (e) Hixson–Crowell and (f) Korsmeyer–Peppas models. Error bars represent standard deviation ($n = 3$).

pH-sensitive swelling behavior of the matrices as explained in the previous sections. Moreover, in both release media, the neat hydrogel released drugs at higher quantities than the corresponding magnetite hybrid hydrogel. It can be seen that after 6 h, the release profile of the neat hydrogel reached nearly equilibrium. In contrast, the magnetite hybrid hydrogel release

profile was nearly equilibrium after 10 h. The decrease in CDR for the magnetite hybrid hydrogel can be explained as follows. The presence of Fe_3O_4 nanoparticles in the gel structure acts as a barrier, creating a denser network and enhancing mechanical strength.[41] This causes an increase in the time required for the medium to penetrate, swelling of the matrices and subsequent dissolution and diffusion of the drug molecules from the matrices to the dissolution medium. It should be noted that the Fe_3O_4 nanoparticles present in the gel structure play an effective role in the time spent for the drug release. While the reduced release rate may appear to be a limitation, it is, in fact, advantageous for controlled drug delivery, as it minimizes burst release and enables prolonged therapeutic action. Furthermore, a higher cumulative release of 5-FU than CUR is attributable to differences in solubility of the drug molecules. In aqueous environments, 5-FU is more soluble than the CUR, dissolving quickly and diffusing out of the matrices. Although encapsulating CUR within the hydrogel matrix improves its apparent solubility and stability, its inherently low bioavailability remains a critical limitation, requiring further pharmacokinetic evaluation.

Generally, the observed pH sensitivity and slow drug release profiles of the magnetite hybrid hydrogel make it a promising drug delivery system for the prolonged treatment of cancer *via* sustained oral dual release of 5-FU and CUR. This study distinguishes itself from previous studies by employing sequential drug release of 5-FU and CUR, which is rarely reported in the literature, particularly for magnetite-based hybrid polymer matrices. Regardless of differences in release approaches, the results obtained in the present study and those reported in the literature are comparable, as summarized in Table 3. The observed pH-dependent, sustained release *via* the sequential release approach, as addressed earlier, strongly differentiates this system from several magnetite-based hydrogels that employed a non-sequential release strategy. These features collectively demonstrate the significance of the present study in advancing multifunctional magnetite hybrid hydrogel-based drug delivery systems.

The drug release kinetics and mechanism describe the properties of the drug delivery system. The diffusion of the drug and degradation of the system are among the main drug release processes. To evaluate the kinetics and mechanism of drug release, various mathematical models, as represented by eqn (8)–(12) have been taken into consideration.[27]

Zero-order kinetic model

$$\frac{Q_t}{Q_\infty} = k_0 t \tag{9}$$

First-order kinetic model

$$\log\left(1 - \frac{Q_t}{Q_\infty}\right) = -\frac{k_1 t}{2.303} \tag{10}$$

Higuchi square root model

$$\frac{Q_t}{Q_\infty} = k_H t^{1/2} \tag{11}$$

Hixson–Crowell model

$$\left(\frac{Q_t}{Q_\infty}\right)^{1/3} = k_C t \tag{12}$$

Korsmeyer–Peppas model

$$\ln\left(\frac{Q_t}{Q_\infty}\right) = \ln(k_P) + n(\ln(t)) \tag{13}$$

where k_0, k_1, k_H, k_C and k_P stand for the rate constant and Q_t/Q_∞ drug release fraction at a predetermined time.

The zero-order kinetic model indicates that the drug is released at a constant rate. The first-order kinetic model indicates that the drug is distributed within the porous matrix, and the rate of drug release depends on the amount of the drug incorporated into the system. In the Higuchi square root model, the release rate is driven by both diffusion and dissolution of the drug. In the Hixson–Crowell model, the drug release rate depends on the system level.[27,41] The Korsmeyer–Peppas model offers the diffusion coefficient (n), which indicates the type of drug transport mechanism from the system to the dissolution medium. If $n \leq 0.5$, the drug transport mechanism adheres to a Fickian diffusion. If $0.5 < n < 1.0$, the transportation of the drug follows a non-Fickian diffusion. If $n = 1.0$, the drug release transport mechanism corresponds to Case II transport. Finally, if $n > 1$, the drug transport mechanism adheres to Super Case II transport.[27] The parameters for the release of 5-FU and CUR from both neat and magnetite hybrid hydrogel are presented in Fig. 6b–f and Table 4. According to the findings, the kinetic behavior of drug release from the matrices into the dissolution medium was best explained by the First-order kinetic model rather than the zero-order kinetic model. The release mechanism adhered to the Korsmeyer–Peppas model and the Higuchi square root model for 5-FU and CUR respectively. Further, the values of 'n' obtained from the Korsmeyer–Peppas model vary significantly. This may be due to several factors, including release conditions, nature of the drugs and composition of the matrices. In particular, at pH 7.4 (a higher-release medium), the release of 5-FU from the nanocomposite followed non-Fickian diffusion ($0.5 < n < 1.0$), indicating that drug release was governed by a combination of diffusion and polymer chain relaxation. In contrast, the release of CUR was best described by Super Case II transport ($n > 1.0$), which is typically associated with swelling-controlled release and significant polymer relaxation. These findings imply that the nanocomposite does not behave as a purely diffusion controlled system; rather, the release of 5-FU and CUR was influenced by the dynamic swelling behavior of the polymer network at pH 7.4. This dual mechanism is advantageous for controlled drug delivery, as it enables sustained and responsive release profiles.

Moreover, the release behavior of 5-FU and CUR from the magnetite hybrid hydrogel strongly correlates with the structural characteristics of the matrix. Firstly, the hydrophilic polymer

Table 3 Comparative release efficiency of the present study and the existing literature

S/N	System	Release approach	Release efficiency	Ref.
1	Chitosan-based reduced graphene oxide nanocomposite	*In vitro*, non-sequential	≈90% of 5-FU and less than 70% of CUR within 72 h	42
2	Xylan–β-cyclodextrin-based hydrogel	*In vitro*, non-sequential	56% 5-FU and 37% CUR during 24 h	43
3	Pectin-*graft*-poly(4-acryloylmorpholine)-based silver nanocomposite hydrogel	*In vitro*, non-sequential	93.9% of 5-FU and 72.2% of CUR	26
4	Diphynylacarbonate crosslinked-β-cyclodextrin-based nanosponges	*In vitro*, non-sequential	≈66.4% of 5-FU and 73.1% of CUR during 24 h	44
5	Chitosan-based reduced graphene oxide/palladium nanocomposites	*In vitro*, non-sequential	≈80% of 5-FU and less than 70% of CUR within 72 h	45
6	Trimethylchitosan/carboxymethylkaraya gum -based nanocomposite silver nanocomposite polyelectrolyte complex	*In vitro*, non-sequential	95.20% of 5-FU and 83.77% of CUR during 24 h	46
7	Chitosan-based hydroxylated boron nitride nanocomposites	*In vitro*, non-sequential	≈96% of 5-FU and less than 84% of CUR within 72	47
8	**Xanthan gum-*graft*-poly(*N*-hydroxyethyl acrylamide)-based iron magnetite nanocomposite hydrogel**	***In vitro*, sequential**	**79% of 5-FU and 56% of CUR during 48 h**	**This study**

Table 4 Drug release parameters for the prepared polymer matrix materials

			XG-*g*-PHEA-2@5-FU/CUR		XG-*g*-PHEA-2/Fe_3O_4@5-FU/CUR	
Model	Parameter	Release medium	5-FU	CUR	5-FU	CUR
Zero-order kinetics	R^2	pH 1.2	0.97	0.93	0.96	0.94
		pH 7.4	0.60	0.70	0.97	0.96
First-order kinetics	R^2	pH 1.2	0.99	0.96	0.99	0.98
		pH 7.4	0.92	0.94	0.99	0.99
Higuchi square root	R^2	pH 1.2	0.95	0.91	0.93	0.94
		pH 7.4	0.88	0.89	0.98	0.99
Hixson–Crowell	R^2	pH 1.2	0.69	0.82	0.73	0.91
		pH 7.4	0.54	0.63	0.90	0.97
Korsmeyer–Peppas	R^2	pH 1.2	0.99	0.86	0.99	0.86
		pH 7.4	0.67	0.87	0.96	0.97
	n	pH 1.2	0.77	1.37	0.91	1.60
		pH 7.4	0.36	0.51	0.67	1.13
	Drug mobility	pH 1.2	Non-Fickian	Super case II	Non-Fickian	Super case II
		pH 7.4	Fickian	Non-Fickian	Non-Fickian	Super case II

matrix enables significant water uptake, leading to swelling and subsequent relaxation of the polymer chains, thereby facilitating drug diffusion. Secondly, as explained earlier, incorporating Fe_3O_4 nanoparticles introduces additional physical crosslinking points within the network, thereby increasing structural integrity and reducing chain mobility. This dual effect (swelling-induced relaxation and nanoparticle-reinforced network rigidity) creates a coupled transport mechanism in which both diffusion and polymer relaxation contribute to drug release. Consequently, the observed non-Fickian behavior arises from this relationship, while the tendency toward Super Case II transport can be attributed to dominant swelling and polymer relaxation at higher hydration levels. However, the reduced swelling in acidic pH and the enhanced structural rigidity imparted by magnetite nanoparticles shift the system toward a more diffusion controlled process, slowing drug release, as supported by the decrease in the values of 'n' from pH 7.4 to pH 1.2. These findings demonstrate that the release profile was not solely diffusion controlled but was critically dependent on the balance between hydrogel

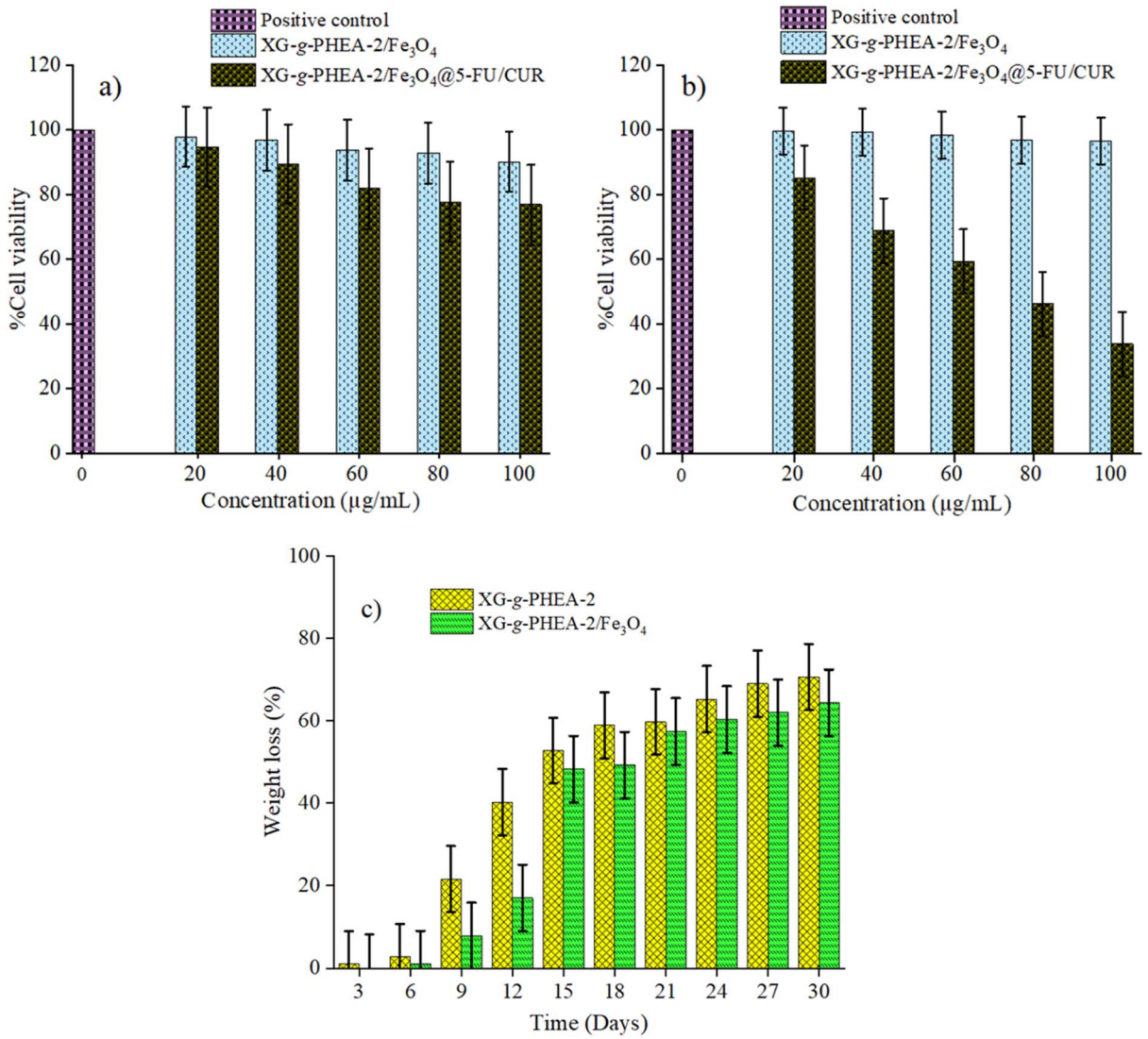

Fig. 7 Viability of (a) MCF-10A and (b) MCF-7 cell lines during 24 h; (c) *in vitro* degradation. Error bars represent standard deviation ($n = 3$).

swelling, network structure, and magnetite-induced reinforcement.

3.6. *In vitro* cytotoxicity and degradation

Cell viability was evaluated for both blank and drug-loaded magnetite hybrid hydrogels against MCF-10A and MCF-7 cells, and the results are depicted in Fig. 7a and b. The primary goal was to assess the cytocompatibility of the developed matrices with and without drugs. Therefore, a blank nanocomposite hydrogel was included as a control to confirm that the observed cytotoxic effects arise from the loaded drugs rather than the vehicle itself. The blank magnetite hybrid hydrogel exhibited no significant toxicity, with cell viability above 90% in both cell lines, even at the highest tested concentration of 100 μg mL^{-1}. In contrast, the drug-loaded magnetite hybrid hydrogel displayed lower cell survival than the blank magnetite hybrid hydrogel. At the end of the study, the cell viability of the drug-loaded magnetite hybrid hydrogel was approximately 77% for the MCF-10A cells and 34% for the MCF-10 cells. The low cell viability for the drug-loaded sample against MCF-7 cells was mainly due to the incorporated anticancer drugs. These results indicate the cytocompatibility of the prepared magnetite hybrid hydrogel with normal cells and its strong inhibitory effect on cancer cells. Although free drug controls were not included in this study, previous reports have shown that 5-FU and CUR exhibit synergistic effects on cancer cells.[48,49] Mechanistically, 5-FU inhibits thymidylate synthase, thereby disrupting deoxyribonucleic acid synthesis and inducing apoptosis in rapidly proliferating cancer cells. CUR, on the other hand, has been widely reported to modulate multiple signaling pathways, including the induction of oxidative stress and activation of apoptotic cascades. The co-delivery of these anticancer drugs may result in synergistic anticancer effects, enhancing cytotoxicity toward MCF-7 cells. Furthermore, the hydrogel-based delivery system likely improves therapeutic efficacy compared to free drugs by enabling sustained, localized release, thereby

enhancing cellular uptake and maintaining effective drug concentrations over time. Previous studies showed that free 5-FU exhibits rapid diffusion and systemic toxicity,[24] whereas CUR suffers from poor solubility and bioavailability.[50] In contrast, encapsulation within polymer matrices has been reported to improve drug stability and therapeutic efficacy.[46,51] Although the present study does not include direct mechanistic assays, the observed selective cytotoxicity strongly suggests apoptosis-mediated cell death.

The Fe_3O_4 nanoparticle-containing hydrogel showed slower degradation than the neat hydrogel, with about 65% of the magnetite hybrid hydrogel degraded within 30 days. During the same period, about 71% of the neat hydrogel degraded. Incorporating Fe_3O_4 nanoparticles into the gel structure reduced the degradation rate by increasing the crosslinking density, as discussed in the previous sections. This is supported by the rapid degradation observed for the neat hydrogel during the first 12 days, compared with that of the magnetite hybrid hydrogel.

However, at the end of the study, there were no drastic changes in weight loss among the samples (Fig. 7c), suggesting that the physical crosslinking between Fe_3O_4 nanoparticles and polymer matrices disrupted during degradation. The degradation trend observed in the present study matches that reported in previous studies.[24,26] Regardless of the observed prolonged degradation, these results suggest that a large portion of the developed material may degrade under physiological conditions, reducing the risk associated with its failure to degrade.

4. Conclusion

In this study, a pH-sensitive XG-*g*-PHEA-2/Fe_3O_4 magnetite hybrid hydrogel was prepared as a potential vehicle for the oral dual drug delivery of 5-FU and CUR. Structural features were evaluated using FTIR, SEM, EDS, XRD and VSM techniques. Swelling studies revealed that the developed magnetite hybrid hydrogel was highly sensitive to the pH. The drug loading and *in vitro* release studies showed that the developed magnetite hybrid hydrogel exhibits slow release of the loaded drugs in acidic conditions of pH 1.2, as simulated gastric fluid. In comparison, its release was rapid in slightly alkaline conditions of pH 7.4, as simulated intestinal fluid. The release kinetics were also evaluated by employing various mathematical models and the release profile was best fitted to the first-order kinetic model. Additionally, the release mechanism followed the Korsmeyer–Peppas model for 5-FU and the Higuchi square root model for CUR. The results from the MTT assay indicate the good cytocompatibility of the developed materials with MCF-10A cells, and the desired cytotoxicity of the drug-loaded magnetite hybrid hydrogel against MCF-7 cells. The pH sensitivity of the material primarily governed the performance of the developed magnetite hybrid hydrogel. Changes in pH may limit the efficiency and effectiveness of materials for drug delivery, affecting drug bioavailability and overall therapeutic effects. Based on the obtained results, the developed magnetite hybrid hydrogel is highly recommended for pH-sensitive dual delivery of 5-FU and CUR, with potential for site-specific release in the gastrointestinal tract. Despite the promising results obtained, this study is a proof of concept, and further studies are required to establish its translational relevance. Firstly, further optimization of the magnetite hybrid hydrogel system is required to precisely control the structural network, swelling behavior, and drug release kinetics. In particular, tuning the interaction between Fe_3O_4 nanoparticles and the polymer matrix could enable more predictable and stimuli-responsive drug delivery. Secondly, to evaluate the relative efficacy of the prepared system compared with free drugs, and to conduct detailed mechanistic studies to elucidate pathways of cell death, including apoptosis, cell cycle arrest, and oxidative stress. Thirdly, *in vivo* studies are recommended to evaluate the actual pharmacokinetics, biodistribution, and therapeutic efficacy of the system under physiological conditions. Fourthly, challenges related to large-scale production, long-term stability, and reproducibility of the hydrogel system need to be addressed by further optimizing the reactive components, as mentioned earlier, to ensure consistent material properties during scale-up. Lastly, the magnetic properties of Fe_3O_4 nanoparticles on externally triggered drug release and targeted delivery using magnetic fields are required to strengthen their role and significance in drug delivery applications.

Conflicts of interest

There are no conflicts to declare.

Data availability

Data will be made available on request.

Acknowledgements

This research is funded by The University of Dodoma under the Junior Academic Staff (JAS) Project Fund. The authors thank The University of Dodoma for financial support, and Infinite Biotech Institute of Research and Analytics, Sangli, Maharashtra, India for providing cytotoxicity analyses.

References

1 T. Y. Tu, S. J. Yang, M. H. Tsai, C. H. Wang, S. Y. Lee, T. H. Young and M. J. Shieh, *Colloids Surf., B*, 2019, **173**, 788–797.
2 A. Saito, J. Kitayama, R. Nagai and K. Aizawa, *Pharmaceutics*, 2023, **15**, 1664.
3 R. Mohammadi, A. Saboury, S. Javanbakht, R. Foroutan and A. Shaabani, *Eur. Polym. J.*, 2021, **153**, 110500.
4 P. Mathur, S. Rawal, B. Patel and M. M. Patel, *Curr. Drug Metab.*, 2019, **20**, 1132–1140.
5 A. Luanda and V. Badalamoole, *Int. J. Biol. Macromol.*, 2023, **228**, 794–807.
6 P. Das, S. Ganguly, A. Saravanan, S. Margel, A. Gedanken, S. Srinivasan and A. R. Rajabzadeh, *ACS Appl. Bio Mater.*, 2022, **5**, 5617–5633.
7 D. Atila and V. Kumaravel, *Biomater. Sci.*, 2023, **11**(20), 6711–6747.

8 S. Dong, S. An, Q. Saiding, Q. Chen, B. Liu, N. Kong, W. Chen and W. Tao, *Chem. Rev.*, 2025, **125**, 8835–8920.
9 L. Xu, L. Qiu, Y. Sheng, Y. Sun, L. Deng, X. Li, M. Bradley and R. Zhang, *J. Mater. Chem. B*, 2018, **6**, 510–517.
10 M. Karimi, M. Eslami, P. Sahandi-Zangabad, F. Mirab, N. Farajisafiloo, Z. Shafaei, D. Ghosh, M. Bozorgomid, F. Dashkhaneh and M. R. Hamblin, *WIREs Nanomed. Nanobiotechnol.*, 2016, **8**, 696–716.
11 S. Ganguly, P. Das, E. Itzhaki, E. Hadad, A. Gedanken and S. Margel, *ACS Appl. Mater. Interfaces*, 2020, **12**, 51940–51951.
12 Y. Liu, L. Dong, Y. Li, Q. Chen, L. Wang, M. A. Farag, L. Liu, S. Zhan, Z. Wu and L. Liu, *Food Hydrocoll.*, 2023, **143**, 108901.
13 K. Hemmati and M. Ghaemy, *Int. J. Biol. Macromol.*, 2016, **87**, 415–425.
14 Y. Zhang, L. Dong, L. Liu, Z. Wu, D. Pan and L. Liu, *J. Agric. Food Chem.*, 2022, **70**(21), 6300–6316.
15 S. Rosalam and R. England, *Enzyme Microb. Technol.*, 2006, **39**, 197–207.
16 A. Rahmatpour and A. H. Alizadeh, *Int. J. Biol. Macromol.*, 2024, **266**, 131394.
17 K. Kashaudhan, P. P. Pande, J. Sharma, R. Shankar and A. Nath, *Environ. Prog. Sustain. Energy*, 2024, **43**, e14419.
18 A. Y. Patne, K. Akramuddaula, D. Patel, M. Suryawanshi and K. Vinchurkar, in *Innovative Pharmaceutical Excipients: Natural Sources*, Springer, Singapore, 2025, pp. 249–298.
19 V. Choudhari, S. Polshettiwar, G. Choudhari and N. S. Topare, in *Handbook of Nanofillers*, Springer, Singapore, 2025, pp. 1581–1615.
20 P. L. Maria Linsha, K. Priya, A. S. Cheriyan and J. T. Varkey, in *Biopolymer-Based Metal Nanoparticles: Synthesis and Applications*, Springer, Singapore, 2025, pp. 99–131.
21 A. Viteri, J. Laugé, L. Lutz, M. P. Ginebra and J. García-Torres, *Int. J. Biol. Macromol.*, 2025, **319**, 145380.
22 S. Barkhordari and A. Alizadeh, *Polym. Bull.*, 2022, **79**, 5533–5548.
23 A. Karimi-Rastehkenari, L. Youseftabar-Miri, E. Askarizadeh and F. Divsar, *Int. J. Biol. Macromol.*, 2025, **319**, 145211.
24 A. Luanda, M. Mahadev, R. N. Charyulu and V. Badalamoole, *Int. J. Biol. Macromol.*, 2024, **282**, 137097.
25 A. Luanda, M. Manohar, R. N. Charyulu and V. Badalamoole, *Int. J. Biol. Macromol.*, 2024, **268**, 131783.
26 A. Luanda, M. Mahadev, R. N. Charyulu and V. Badalamoole, *Macromol. Chem. Phys.*, 2025, **226**, 2400428.
27 A. Luanda, M. Mahadev, R. N. Charyulu and V. Badalamoole, *Polym. Adv. Technol.*, 2025, **36**, 1–16.
28 S. Shruthi and B. Vishalakshi, *Int. J. Biol. Macromol.*, 2024, **278**, 134877.
29 F. Paquin, J. Rivnay, A. Salleo, N. Stingelin and C. Silva-Acuña, *J. Mater. Chem. C*, 2015, **3**, 10715–10722.
30 Y. Yue, S. K. Yadav, C. Wang, Y. Zhao, X. Zhang and Z. Wu, *Carbohydr. Polym.*, 2018, **197**, 57–65.
31 S. Rahmani, A. Olad and Z. Rahmani, *Polym. Bull.*, 2023, **80**, 4117–4138.
32 K. S. Sivudu and K. Y. Rhee, *Colloids Surf., A*, 2009, **349**, 29–34.
33 E. A. Fadl, W. A. A. Sadik, A. G. El Demerdash, H. A. Moukhtar and M. E. S. Hamza, *Sci. Rep.*, 2025, **15**, 1–19.
34 M. W. Sabaa, D. H. Hanna, M. H. Abu Elella and R. R. Mohamed, *Mater. Sci. Eng. C*, 2019, **94**, 1044–1055.
35 S. Chami, N. Joly, P. Bocchetta, P. Martin and D. Aliouche, *Polymers*, 2021, **13**, 1484.
36 P. Kulal and V. Badalamoole, *J. Environ. Chem. Eng.*, 2020, **8**, 104207.
37 T. S. Anirudhan, B. Binusreejayan and S. R. Rejeena, *Int. J. Polym. Mater. Polym. Biomater.*, 2014, **63**, 539–548.
38 P. V. S. Rudhrabatla, R. Jalababu, K. S. V. Krishna Rao and K. V. N. Suresh Reddy, *J. Drug Deliv. Sci. Technol.*, 2019, **51**, 438–453.
39 A. B. Suresh, M. R. Rajeev and T. S. Anirudhan, *J. Environ. Chem. Eng.*, 2023, **11**, 109862.
40 E. Tanasa, C. Zaharia, I.-C. Radu, V.-A. Surdu, B. S. Vasile, C.-M. Damian and E. Andronescu, *Nanomaterials*, 2019, **9**, 1384.
41 R. Foroutan, A. Mohammadzadeh, S. Javanbakht, R. Mohammadi and M. Ghorbani, *Results Chem.*, 2025, **15**, 102177.
42 S. Dhanavel, T. A. Revathy, T. Sivaranjani, K. Sivakumar, P. Palani, V. Narayanan and A. Stephen, *Polym. Bull.*, 2020, **77**, 213–233.
43 P. Gami, D. Kundu, S. D. K. Seera and T. Banerjee, *Int. J. Biol. Macromol.*, 2020, **158**, 18–31.
44 H. Mashaqbeh, R. Obaidat, M. M. Alsmadi, S. Bardaweel and N. Hailat, *J. Drug Deliv. Sci. Technol.*, 2024, **99**, 105968.
45 S. Dhanavel, P. Praveena, V. Narayanan and A. Stephen, *Polym. Bull.*, 2020, **77**, 5681–5696.
46 R. Anjar, M. Mahadev, R. N. Charyulu and V. Badalamoole, *J. Mater. Chem. B*, 2025, **13**, 3602–3617.
47 S. Dhanavel, T. Sivaranjani, K. Sivakumar, P. Palani, V. K. Gupta, V. Narayanan and A. Stephen, *J. Iran. Chem. Soc.*, 2021, **18**, 317–329.
48 J. H. Lee, J. H. Park, Y. Jung, J. H. Kim, H. S. Jong, T. Y. Kim and Y. J. Bang, *Mol. Cancer Ther.*, 2006, **5**, 3085–3095.
49 Q. Wang, C. Liang, S. Shen, M. Liu and L. Bai, *Chinese J. Clin. Pharmacol. Ther.*, 2025, **30**, 1122–1126.
50 K. Suresh and A. Nangia, *CrystEngComm.*, 2018, **20**(24), 3277–3296.
51 P. Guo, C. Pi, S. Zhao, S. Fu, H. Yang, X. Zheng, X. Zhang, L. Zhao and Y. Wei, *Expert Opin. Drug Deliv.*, 2020, **17**, 1473–1484.